Boundary-Layer Meteorology

Early-morning flow transition in a valley in low-mountain terrain

--Manuscript Draft--

Manuscript Number:	
Full Title:	Early-morning flow transition in a valley in low-mountain terrain
Article Type:	Research Article
Keywords:	Convection in a valley; Coherent structures; Large-eddy simulation; Energy balance closure; COPS
Corresponding Author:	Bjoern Broetz, Dipl.-Met. DLR Weßling, GERMANY
Corresponding Author Secondary Information:	
Corresponding Author's Institution:	DLR
Corresponding Author's Secondary Institution:	
First Author:	Bjoern Broetz, Dipl.-Met.
First Author Secondary Information:	
Order of Authors:	Bjoern Broetz, Dipl.-Met.
	Rafael Eigenmann, Dipl.-Geoökol.
	Andreas Dörnbrack, Dr.
	Thomas Foken, Prof. Dr.
	Volkmar Wirth, Prof. Dr.
Order of Authors Secondary Information:	
Abstract:	This study investigates the evolution of the early-morning boundary layer in a low-mountain valley in south-western Germany during the Convective and Orographically induced Precipitation Study (COPS) in summer 2007. A subset of 23 fair weather days of the campaign was selected to study the transition of the boundary-layer flow in the early morning. The typical valley atmosphere in the morning hours was characterized by a stable temperature stratification and a pronounced valley wind system. During the reversal period - named as low wind period - of the valley wind system (duration of 1-2 hours), the horizontal wind was very weak and the conditions for free convection were fulfilled close to the ground. Ground-based Sodar observations of the vertical wind showed enhanced values of upward motion, and the corresponding statistical properties differ from those observed under windless convective conditions over flat terrain. Large-eddy simulations of the boundary-layer transition in the valley were conducted. Statistical properties of the simulated flow agree with the observed quantities. Spatially coherent turbulence structures are present in temporal as well as in ensemble mean analysis. Thus, the complex orography forms coherent convective structures at predictable, specific locations during the early-morning low wind situations. These coherent updraughts - found in both the Sodar observations and the simulation - lead to a flux counter to the gradient of the stably stratified valley atmosphere and reach up to the heights of the surrounding ridges. Furthermore, the energy balance in the surface layer in the low wind periods is closed. However, it becomes unclosed after the onset of the valley wind. The partition into the sensible and the latent heat fluxes indicates that missing flux components of sensible heat are the main reason for the unclosed energy balance in the considered situations. This result supports previously published investigations on the energy balance closure.
Suggested Reviewers:	Matthias Rotach, Prof. Dr. Professor for Dynamic Meteorology, University of Innsbruck mathias.rotach@uibk.ac.at

Powered by Editorial Manager® and Preprint Manager® from Aries Systems Corporation

	Expert in mountain meteorology
	Werner Eugster, PD Dr. Senior Scientist, ETH Zürich werner.eugster@ipw.agrl.ethz.ch Expert in micrometeorology
	Edward Patton, Dr. Project Scientist, NCAR patton@ucar.edu Expert in boundary meteorology Expert in Large-Eddy Simulations
	Roland Vogt, Dr. Senior Scientist, University of Basel roland.voigt@unibas.ch Expert in Eddy-Covariance MeasurementsExpert in boundary-layer meteorology
	Reinhold Steinacker, Prof. Dr. Head of Department, Universität Wien reinhold.steinacker@univie.ac.at Expert in Boundary-Layer Meteorology
	Christoph Kottmeier, Prof. Dr. Head of Department, Karlsruhe Institute of Technology christoph.kottmeier@kit.edu Expert in Meteorology
	Ulrich Corsmeier, Dr. Group leader, Karlsruhe Institute of Technology ulrich.corsmeier@kit.edu Expert in Boundary-layer Meteorology

Powered by Editorial Manager® and Preprint Manager® from Aries Systems Corporation

Manuscript
Click here to download Manuscript: Broetz_et_al_20130107.tex
Click here to view linked References

Boundary Layer Meteorology manuscript No.
(will be inserted by the editor)

Early-morning flow transition in a valley in low-mountain terrain

Björn Brötz · Rafael Eigenmann · Andreas Dörnbrack · Thomas Foken · Volkmar Wirth

Received: date / Accepted: date

Abstract This study investigates the evolution of the early-morning boundary layer in a low-mountain valley in south-western Germany during the Convective and Orographically induced Precipitation Study (COPS) in summer 2007. A subset of 23 fair weather days of the campaign was selected to study the transition of the boundary-layer flow in the early morning. The typical valley atmosphere in the morning hours was characterized by a stable temperature stratification and a pronounced valley wind system. During the reversal period - named as low wind period - of the valley wind system (duration of 1-2 hours), the horizontal wind was very weak and the conditions for free convection were fulfilled close to the ground. Ground-based Sodar observations of the vertical wind showed enhanced values of upward motion, and the corresponding statistical properties differ from those observed under windless convective conditions over flat terrain. Large-eddy simulations of the boundary-layer transition in the valley were conducted. Statistical properties of the simulated flow agree with the observed quantities. Spatially coherent turbulence structures are present in temporal as well as in ensemble mean analysis. Thus, the complex orography forms coherent convective structures at predictable, specific locations during the early-morning low wind situations. These coherent updraughts - found in both the Sodar observations and the simulation - lead to a flux counter to the gradient of the stably stratified valley atmosphere and reach up to the heights of the surrounding ridges. Furthermore, the energy balance in the surface layer in the low wind periods is closed. However, it becomes unclosed after the onset of the valley wind. The partition into the sensible and the latent heat fluxes indicates that

B. Brötz · V. Wirth
University of Mainz, Institute for Atmospheric Physics, 55099 Mainz, Germany

Present address of B. Brötz:
Deutsches Zentrum für Luft- und Raumfahrt, Institut für Physik der Atmosphäre, Oberpfaffenhofen, Germany
E-mail: Bjoern.Broetz@dlr.de

A. Dörnbrack
Deutsches Zentrum für Luft- und Raumfahrt, Institut für Physik der Atmosphäre, Oberpfaffenhofen, Germany

R. Eigenmann · T. Foken
University of Bayreuth, Department of Micrometeorology, 95440 Bayreuth, Germany

T. Foken
Bayreuth Center of Ecology and Environmental Research (BayCEER), 95440 Bayreuth, Germany

missing flux components of sensible heat are the main reason for the unclosed energy balance in the considered situations. This result supports previously published investigations on the energy balance closure.

Keywords Convection in a valley · Coherent structures · Large-eddy simulation · Energy balance closure · COPS

1 Introduction

Turbulent fluxes of heat, moisture, and momentum in the atmospheric boundary layer are of key importance both for the evolution of the boundary layer itself and for the overlying free atmosphere. The accurate knowledge of the magnitude and the vertical profiles of these fluxes and their reliable parametrization are essential for both numerical weather prediction and climate simulations, respectively. Sophisticated micrometeorological instrumentation and analysis techniques have successfully been applied in order to determine fluxes over flat and homogeneous terrain.

However, the determination of these fluxes above complex terrain, i.e. mountainous and/or with heterogeneity in land use, remains a challenging task (Foken, 2008; Mahrt, 2010). The boundary layer in complex terrain is characterized by orographically (Defant, 1949; Whiteman, 1990; Whiteman, 2000; Zardi and Whiteman, 2013) or thermally induced (Segal and Arritt, 1992) wind systems. In a convective boundary layer over flat surfaces quasi-stationary turbulence structures evolve (Schmidt and Schumann, 1989). Over heterogeneous surfaces (Dörnbrack and Schumann, 1993; Walko et al., 1992) coherent structures with surface-scale dependent length scales develop, especially in the lower part of the boundary layer. These flow structures can potentially modify the turbulent fluxes from valleys, thus potentially modifying the evolution of the mountainous boundary layer as a whole. Rotach et al. (2008) and Weigel et al. (2007) investigated the exchange processes in an alpine valley and found strong dependencies of the turbulent fluxes on orography and stratification in the mountainous boundary layer. Mayer et al. (2008) investigated an observed anomaly in the chemical composition of air at a mountain station. This anomaly was traced back to fluxes through the stably stratified valley atmosphere that were released during the reversal of the thermally driven wind system in the morning.

Over homogeneous terrain a strong influence of coherent turbulent structures, i.e. persistent quasi-stationary patterns of turbulent motion, on the turbulent fluxes was shown in several studies (Raasch and Harbusch, 2001; Kanda et al., 2004; Inagaki et al., 2006). In particular, the interpretation of micrometeorological measurements in complex terrain requires the comprehensive knowledge about how turbulence is organized at the observational site and its surrounding. This leads to the guiding questions for this study: (i) How does the convective boundary layer in a typical low-mountain valley get organized in the early morning hours after sunrise? (ii) How does an along-valley wind in the morning change the convective structures? (iii) To what extent is the vertical transport in the valley affected? (iv) How are micrometeorological flux measurements at a specific location affected by complex terrain? To address these questions, large-eddy simulations (LES) were conducted. The results of the simulations are compared to observations.

A unique dataset obtained during the field phase of COPS constitutes the basis of this study (see Eigenmann et al., 2009). The field campaign of summer 2007 in the low-mountain region of south-western Germany and eastern France, i.e. Black Forest and Vosges mountains, is well described in the literature (e.g. Wulfmeyer et al., 2011). The objective of the campaign is to understand the influence of the orography of a low-mountain range on precipitation. Several surface flux measurement stations were installed throughout the respective region during the campaign (Eigenmann et al., 2011; Kalthoff et al., 2011). In addition, ground-based Sodar/RASS instruments were installed on some of these stations. Our study uses data from one of these sites where a full energy balance station and a Sodar/RASS operated simultaneously. The site Fußbach is located in the Kinzig valley, which is a typical low-mountain valley of the region with a pronounced valley wind system developing on fair weather days in summer.

In micrometeorological field experiments the energy balance is often not closed (e.g. Oncley et al., 2007; Foken et al., 2010). Although many uncertainties are connected with the determination of the components of the energy balance (Mahrt, 2010), strong indications exist that the residual occurs due to transport by large-scale eddies or secondary circulations which are not captured by the eddy-covariance method (e.g. Mauder and Foken, 2006; Foken, 2008; Foken et al., 2010, 2011; Stoy et al., 2013). As these secondary circulations are mainly associated with the buoyancy flux, the partitioning of the residual according to the buoyancy flux ratio approach, proposed by Charuchittipan et al. (2013), appears to be appropriate to close the energy balance. The buoyancy flux ratio approach partitions the residual according to the buoyancy flux ratio instead of the usually used Bowen ratio (Twine et al., 2000). Thus, a larger fraction of the residual would be attributed to the sensible heat flux with the buoyancy flux ratio approach. Also the COPS energy balance site Fußbach of this study shows an average residual of 21% during the entire field campaign (see Eigenmann et al., 2011).

The remainder of this article is organized as follows. Section 2 describes the data and the methods applied, in particular the numerical model and its set-ups. Section 3 presents the results and the discussion of them. The conclusions are given in Sect. 4.

2 Methods and data

2.1 Observational data

The data used in this study were obtained by observations conducted during the COPS experiment in the low-mountain terrain of the Kinzig valley. Turbulence data were measured at a height of 2 m above the valley surface and friction velocity u_*, sensible heat Q_H and latent heat Q_E were calculated with the eddy-covariance method (EC) (Foken et al., 2012). An averaging time of 30 min was used for the EC. Contributions to the fluxes with a time scale exceeding these 30 min cannot be captured. The geographical location of the site Fußbach was 48° 22′ 7.8″ N, 8° 1′ 21.2″ E, 178 m a.s.l. (the position is marked in Fig. 3). The local time is UTC+1 hour. Details about the site and the measurement set-up can be found in Metzger et al. (2007) and Eigenmann et al. (2009, 2011). Close to the turbulence station, a Sodar/RASS system measured vertical profiles of wind components and virtual temperature. Moreover, the remaining components of the energy balance, net radiation Q_S^*, and soil heat flux Q_G, were measured at the EC site. An overview of the data processing, quality control, and flux characteristics of the turbulent data as well as the calculation of the energy balance is given in Eigenmann et al. (2011).

The study of Eigenmann et al. (2009) identified 23 days during the three-month COPS campaign with free convective conditions based on the EC measurements in the early-morning hours. Free convective conditions were identified by the stability parameter $\zeta = zL^{-1}$ for $\zeta < -1$, where L is the Obukhov length. These periods were characterized by low horizontal wind due to the reversal of the valley wind system from down-valley winds to up-valley winds. The mean time of the occurrence of the free convective situations on these 23 days is 0815 UTC with a standard deviation of 1 hour.

The vertical wind speed w derived from the Sodar observations was analysed for the identified low wind periods. In the remainder of the article this period of low wind will be referred to as p_1 and the subsequent period of up-valley wind will be referred to as p_2. In order to make the individual days comparable, each Sodar sample of w was normalized with the Deardorff convective velocity w_* (Deardorff, 1970). The measurement height z was normalized with the height of the boundary layer z_i. Surface buoyancy fluxes for the calculation of w_* were derived from the EC measurements and values of z_i were determined by a secondary maximum in the reflectivity profiles of the Sodar measurements as described in Eigenmann et al. (2009) and suggested by Beyrich (1997). After that, histograms of ww_*^{-1} were calculated for three characteristic heights of $zz_i^{-1} = 0.25, 0.50$ and 0.75.

2.2 Simulations

2.2.1 Numerical Model

The numerical simulations were conducted by means of the multiscale geophysical flow solver EULAG (Smolarkiewicz et al., 1997; Prusa et al., 2008). EULAG solves the non-hydrostatic, anelastic equations of motion, here written in an extended perturbational form (Smolarkiewicz and Margolin, 1997):

$$\nabla \cdot (\rho_b \mathbf{v}) = 0, \tag{1}$$

$$\frac{D\mathbf{v}}{Dt} = -\nabla \pi' - \mathbf{g}\frac{\Theta'}{\Theta_b} + \mathbf{M} + \mathbf{D} + \mathbf{F} - \alpha \mathbf{v}', \tag{2}$$

$$\frac{D\Theta'}{Dt} = -\mathbf{v} \cdot \nabla \Theta_e + \mathscr{H} - \beta \Theta'. \tag{3}$$

$$\frac{De}{Dt} = \mathscr{S} \tag{4}$$

The set of anelastic equations (1)-(4) describes the anelastic mass continuity equation (1), the three components of the momentum equation (2), and the thermodynamic equation (3), respectively. The equation (4) for the subgrid-scale (SGS) turbulent kinetic energy (TKE) e completes the system of equations. In (1)-(4), the operators ∇ and $\nabla\cdot$ symbolize gradient and divergence, while $D/Dt = \partial/\partial t + \mathbf{v} \cdot \nabla$ is the material derivative, and $\mathbf{v}$ is the physical velocity vector. The vector representing the gravitational acceleration $\mathbf{g} = (0, 0, -g)^T$ occurs in the buoyancy term of Equ. (2). The quantities $\rho_b(z)$ and $\Theta_b(z)$ refer to the basic states, prescribed hydrostatic reference profiles usually employed in the anelastic approximated equations (Clark and Farley, 1984).

In addition to the horizontally homogeneous basic state, a more general ambient (environmental) state is denoted by the subscript $_e$. The corresponding variables may vary in the horizontal directions and they have to satisfy Equ. (1)-(3); see Prusa et al. (2008) for a discussion of ambient state and its benefits. The primed variables $\mathbf{v}'$ and Θ' appearing in Equ. (2)-(3) correspond to deviations from the environmental variables $\mathbf{v}_e$ and Θ_e. The quantity π' in the linearized pressure gradient term in Equ. (2) denotes a density normalized pressure deviation.

The terms proportional to α and β denote wave absorbing devices used at the upper boundary of the computational domain. The source terms $\mathbf{D}$ and $\mathscr{H}$ not explicitly stated

Table 1 Set-ups for the simulations in this study

name	terrain	stratification below z_i	z_i, (m)	wind forcing	dx, (m)
$S1$	flat	neutral	800	off	20
$S2$	flat	–	0	off	20
$R1$	complex	neutral	800	off	30
$R2$	complex	–	0	on (during p2)	30

in Equ. (2) and (3) symbolize the viscous dissipation of momentum and the diffusion of heat, respectively. **F** symbolizes an additional forcing for specified simulations, see below. The formulation of the TKE production and dissipation term hidden in $\mathscr{S}$ and the applied parameters follow the description of Sorbjan (1996).

The quantity **M** denotes metric forces due to the curvilinearity of the underlying physical system. In the present work, a non-orthogonal terrain-following system of coordinates $(\bar{x},\bar{y},\bar{z}) = (x,y,H(z-h)/(H-h))$ is used which assumes a model depth H and an irregular lower boundary $h(x,y)$ (Gal-Chen and Somerville, 1975; Smolarkiewicz and Margolin, 1993; Wedi and Smolarkiewicz, 2004). The explicit formulation of the transformed system of equations can be found in Prusa and Smolarkiewicz (2003) or, more recently, in Kühnlein et al. (2012). In symbolic form, the resulting system of motion for the prognostic variables $\Psi = u, v, w, \Theta, e$ can be written as a flux-form Eulerian conservation law

$$\frac{\partial}{\partial t}(\rho^* \Psi) + \nabla \cdot (\mathbf{v} \rho^* \Psi) = \rho^* F^{\Psi} \tag{5}$$

where $\rho^* = \rho_b G$, with G as the Jacobian of the transformation. A finite difference approximation of Equ. (5) is

$$\Psi^{n+1} = MPDATA\left(\Psi^n + 0.5\Delta t F^{\Psi}\Big|^{n}, \mathbf{v}^{n+\frac{1}{2}}, \rho^*\right) + 0.5\Delta t \rho^* F^{\Psi}\Big|^{n+1} \tag{6}$$

where MPDATA[1] stands for the non-oscillatory forward-in-time (NFT) advection transport scheme described in Smolarkiewicz and Margolin (1998). The elliptic equation for pressure is solved iteratively with a Krylov-sub space solver, see Thomas et al. (2003). Both elements are integral part of the EULAG and are fundamental for the stability of the code and the reliability of the results.

2.2.2 Simulation strategy

Among the broad range of applications documented in literature, EULAG was successfully applied to atmospheric boundary-layer flows (see Smolarkiewicz et al., 2007; Piotrowski et al., 2009). For the questions investigated in this paper, the set-up was chosen in the following way.

The numerical simulations are conducted in a domain of $(L_x, L_y, H) = (7680\,\text{m}, 7680\,\text{m}, 2430\,\text{m})$ with a regular grid size of $\Delta x = \Delta y = \Delta z = 30\,\text{m}$. For a simulation of 2.5 h physical time, 30 000 timesteps with $\Delta t = 0.3\,\text{s}$ are necessary. The height $h(x,y)$ of the lower boundary is taken from the ASTER digital topographic data set (NASA Land Processes Distributed Active Archive Center NASA LP DAAC, 2001) in a $30\,\text{m} \times 30\,\text{m}$ regular resolution. In all simulations shown here the computational domain is periodic in the horizontal directions. To enable this periodicity the topography was smoothly relaxed within a frame

[1] MPDATA stands for Multidimensional Positive-Definite Advection Transport Algorithm

around the actual region of interest. Due to the complex orography and the low inversion layer height the width of the frame could be chosen to be 300 m.

For all simulations an anelastic basic state with a background stratification $N = 0.01\ \mathrm{s}^{-1}$ is used according to Clark and Farley (1984), resulting in exponentially decreasing ρ_b and increasing Θ_b-profiles.

To investigate the guiding questions of this study, two different simulation set-ups were designed. First, idealized simulations of an evolving convective boundary layer (CBL) over flat terrain $h(x,y) = 0$ were conducted and they are denoted by S, and, secondly, the CBL was simulated over realistic topography $h(x,y)$ and these simulations are denoted by R, see Table 1.

All simulations were initialized with a resting fluid, and two different ambient potential temperature profiles $\Theta_e(z)$ were applied to distinguish between an early mixed layer with a capping inversion layer at $z_i = 800$ m (Simulations $S1$ and $R1$) and a stably stratified ambient state covering the whole depth of the computational domain (simulations $S2$ and $R2$):

$$\text{Simulations } S1 \text{ and } R1: \quad \Theta_e = \begin{cases} \Theta_0 & \text{for} \quad h \leq z < z_i \\ \Theta_0 \left(1 + \frac{N^2}{g}(z - z_i)\right) & \text{for} \quad z_i \leq z \leq H \end{cases} \tag{7}$$

$$\text{Simulations } S2 \text{ and } R2: \quad \Theta_e = \Theta_0 \left(1 + \frac{N^2}{g} z\right) \qquad \text{for} \quad h \leq z \leq H \tag{8}$$

White noise with an amplitude of $0.001\ \mathrm{m\,s^{-1}}$ was added to the initial vertical wind field in order to initiate convective motions. For the ensemble runs analysed in Section 3.2, eight independent realizations were simulated using the set-up $R1$. For this purpose, the random generator was seeded differently at the initial time for each realization. Because the three wind components are zero before adding the noise, the random disturbance is 100 % of the absolute value of the wind vector. This ensures that the eight realizations are statistically independent. The numerical simulations were conducted for a dry atmosphere. At the surface a sensible heat flux $Q_H = 0.05\ \mathrm{K\,m\,s^{-1}}$ was specified in all runs. The homogeneous heating can be justified because flux differences between different types of land surfaces turned out to be negligible in the observed early-morning situations (see Eigenmann et al., 2011). The effect of orographic shading is not taken into account. Orographically-induced flows (valley winds, upslope flows, etc.) are expected to mainly dominate the properties of the CBL in the valley at this time of the day.

During the night-day-transition, the along-valley winds are part of a mountain plain circulation between a mountain massive and an adjacent plane, in our case the Black Forest and the Upper Rhine Valley, respectively. Due to the small computational domain, the effect of this meso-scale circulation on the flow in the valley is modelled by an additional dynamical forcing $\mathbf{F} = (0, -v_0(z)\tau^{-1}, 0)$ for the meridional wind component v, where $\tau = t_{\mathrm{end}} - t_{\mathrm{beg}}$ is the period when the forcing is applied. The reference profile for the horizontal wind speed $v_0(z)$ was derived from the Sodar observations. In the simulation $R2$ the additional forcing $\mathbf{F}$ is applied. The period from $t = 0$ to t_{beg} represents the observed low wind period p_1. The period from t_{beg} to the end of the simulation represents the up-valley wind period p_2. In the remainder of the article two simulation times referred to as t_1 for a time in p_1 and t_2 for a time in p_2 are chosen in order to compare differences in the simulated periods p_1 and p_2.

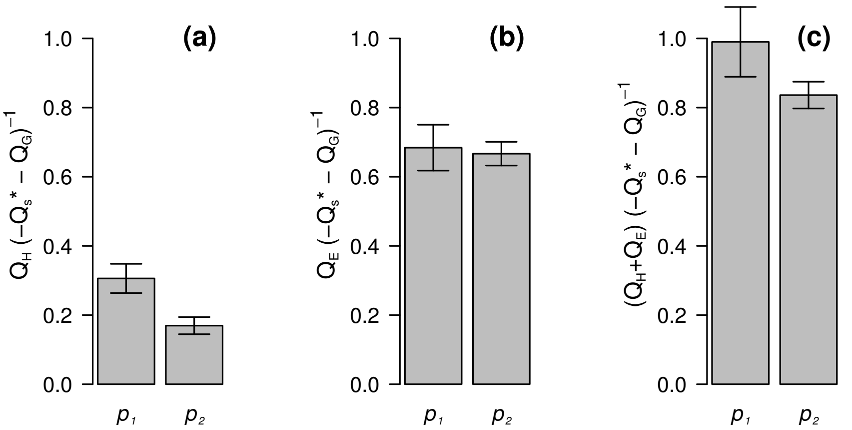

Fig. 1 Bar plots of the mean of the fluxes of Q_H (a), Q_E (b) and the sum of both (c) normalized with the available energy $-Q_S^* - Q_G$ during the low wind speed period p_1 and the first 2 hours of p_2. Average values for the 23 selected days at the Fußbach site are given for both periods. Also shown are the 95% confidence intervals which indicate significant differences in the mean values for (a) and (c).

3 Results and Discussion

3.1 Modification of the energy balance by the valley wind

To analyse the effect of the valley wind on the energy balance of the EC flux measurements, the selected periods p_1 and p_2 are analysed separately. Figure 1 shows the mean of the fluxes Q_H and Q_E and the sum of both normalized with the available energy $-Q_S^* - Q_G$ during the low wind speed period p_1 and the first 2 hours of p_2. This interval was chosen in order to make the data basis of both periods comparable. A closed energy balance means that the ratio of the sum of the turbulent fluxes $Q_H + Q_E$ and the available energy $-Q_S^* - Q_G$ is equal to one. Altogether, the energy balance is closed in p_1, while in p_2 a residual of 16% occurs on average (see Fig. 1c). The latter value is close to the average residual of 21% found during the entire COPS campaign at this site (see Eigenmann et al., 2011).

Regarding Fig. 1a and b, the relative flux contributions missing in period p_2 compared to period p_1 have exactly the proportions of the buoyancy flux ratio. The buoyancy flux ratio would distribute about 85% of the residual to Q_H and 15% to Q_E for a typical Bowen ratio of about 0.45 in the observed early-morning situations. As such, Fig. 1 supports the application of the buoyancy flux ratio approach (see Charuchittipan et al., 2013) for the correction of the energy balance. The missing flux components in period p_2 are assumed to be transported within buoyancy-driven secondary circulations not captured by the EC measurements (e.g. Foken, 2008). The transfer of the missing energy into the secondary circulation mainly happens at significant surface heterogeneities which can be found over complex terrain. Advection-dominated processes (also not captured by the EC) probably lead to the transport of the missing energy to these heterogeneities. As wind speeds vanish in period p_1, no energy is transferred into secondary circulations and the energy balance is closed. However, the along-valley wind in period p_2 leads to missing advective flux components and thus to the observed residual in this period.

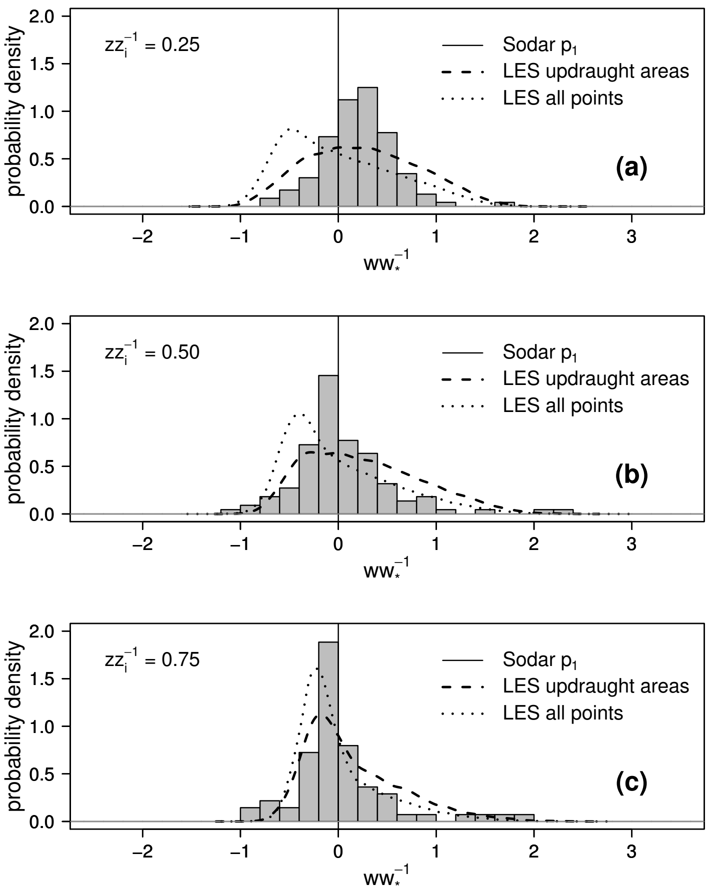

Fig. 2 Probability densities of the normalized vertical wind speed ww_*^{-1} for three heights ($zz_i^{-1} = 0.25, 0.5, 0.75$). Histograms are derived from Sodar observations at the Fußbach site during the low wind speed periods p_1 on the 23 selected days, while curves are derived from the simulation $S2$. The dotted curve shows the probability density function (pdf) for all points in the horizontal plane, the dashed curve shows the pdf for the conditionally sampled updraught areas only.

The finding discussed above also supports the choice of a constant heat flux forcing for the transient simulation $R2$ (see Sect. 2.2). The same relative forcing by Q_H is achieved for both periods p_1 and p_2 by adding (for simplification) 100% of the residual to Q_H. In this way, the forcing of period p_1 can also be used for period p_2. Moreover, no significant relative flux differences of Q_E exist in both periods (see Fig. 1b). Thus, for the questions addressed in this study, it appears to be appropriate to concentrate on dry model runs.

3.2 Coherent structures in the valley imposed by surrounding orography

In order to investigate the early-morning CBL evolution inside the valley, Sodar data from the morning period p_1 of the selected days were chosen to create the histograms of the

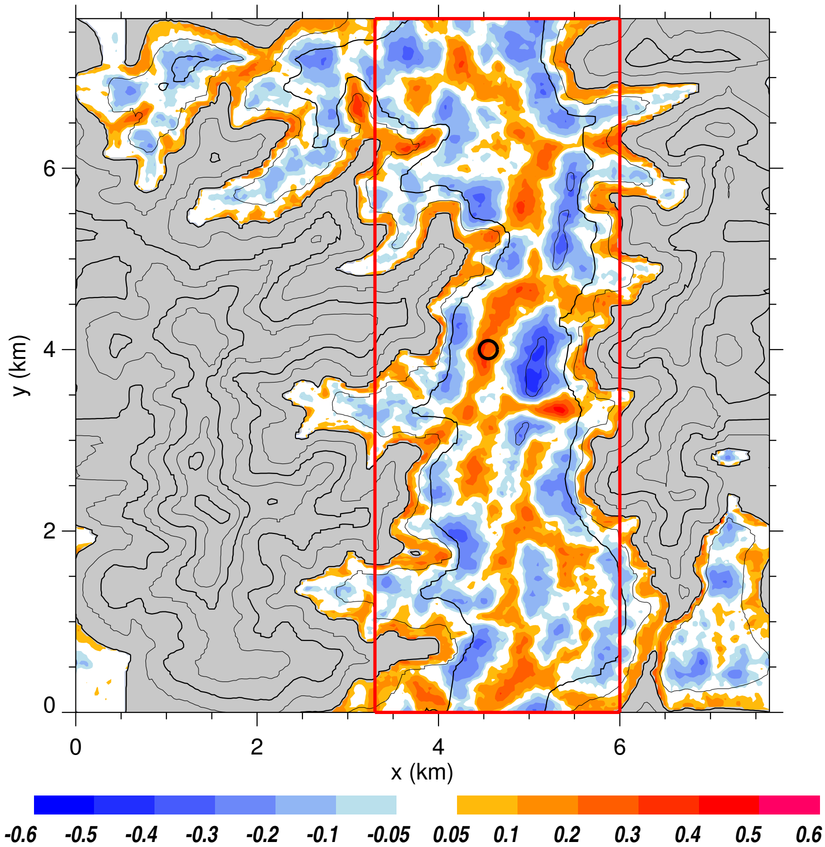

Fig. 3 Ensemble and time mean of the vertical wind speed in m s^{-1} at 300 m a.s.l. for simulation $R1$ (colour-coded). Black solid lines mark the orography in steps of 50 m. Grey contours mark intersection with the orography. The red frame represents the section of the valley shown in Fig. 5. The position of the Sodar is indicated by the black circle.

normalized vertical wind ww_*^{-1} (see Fig. 2). The observed distributions of this study deviate strongly from probability density functions (pdfs) observed over flat, homogeneous environments as reported by many studies (e.g. Deardorff and Willis, 1985; Stull, 1988). In these studies the pdfs are right-skewed and show a negative maximum. Especially in the lower part of the boundary layer ($zz_i^{-1} = 0.25$) the maximum of the observed distribution at Fußbach site is shifted towards weak positive values instead of the weak negative values known from literature. Also the observed histogram is far less skewed at this height. To find the cause of this behaviour, idealized simulations of a CBL are carried out (Simulation $S1$ and $S2$, described in Sect. 2.2).

To gain confidence in the simulations the well known pdfs of the vertical wind in a convective boundary layer are calculated for the simulated data of set-up $S1$. Very good agreement with the published values is found (not shown). Moreover, the simulation results show the well-known spoke patterns of coherent convective motion known from numerous numerical studies (e.g. Schmidt and Schumann, 1989). The data from the simulation of set-up $S2$ is then used to create the pdfs for a CBL with growing mixed layer, see Fig. 2 (situation more close to observation period p_1). In this set-up, spoke patterns evolve in the simulated boundary layer that grow slightly in size as the inversion layer height grows in time. A conditional sampling is applied to obtain the pdfs of the coherent updraught areas.

The resulting pdfs resemble the properties of the histograms from the Sodar data (see Fig. 2). The maximum and the skewness of the pdfs of the conditionally sampled updraught areas match well with those of the histograms of the observational data for all heights. Only the absolute numbers of the probability density do not fully match. A possible explanation for this is that the Sodar instrument averages over a certain volume, so that the probability density of values around zero gets increased. This effect becomes larger with height.

We interpret these findings as follows: It is well known that coherent convective motions evolve in a CBL which remain quasi-stationary in space and time (see e.g. Stull, 1988). This means that the location where a possible Sodar instrument is located will remain under an updraught or a downdraught area for a long time. As a consequence, it is very likely that a Sodar measurement will capture only the statistical properties of a part of the velocity spectrum. The fact that the result from Fig. 2 stems from a composite over 23 periods with similar overall conditions suggests the hypothesis that the Sodar instrument was preferentially located at an updraught region.

To verify this hypothesis, an ensemble of eight large-eddy simulations was carried out with realistic topography at the lower boundary (simulation $R1$) and different initial noise seeding for w (see Sect. 2.2.2). Figure 3 shows the ensemble and time mean of the vertical wind speed at 300 m a.s.l. (approximately 130 m above the valley floor). Although we applied both a temporal mean and an ensemble mean to the simulated data, coherent patterns of the CBL flow field inside the valley remain. This mean flow field has a larger amplitude than its analogue from simulations over flat terrain. We interpret this finding as follows: The surrounding ridges impose coherent convective motions to the valley flow at specific locations during the early-morning p_1 periods. Their positions relative to the ridges persist in contrast to the changing locations of the coherent structures in the flat CBL simulation. The position of the observational site is marked by a black circle in Fig. 3 and shows that the site is located in an updraught region.

3.3 Vertical transport in the early-morning valley atmosphere

Spectral analysis of the EC measurements in the valley showed an increase of spectral power within turbulent scales of a few minutes during the low wind speed period p_1 in the morning (see Eigenmann et al., 2009). These time scales could be related to the presence of large coherent vertical structures (e.g. plumes or updraughts) with a spatial extent in the order of the boundary-layer height, which are known to be responsible for the majority of the transport within the CBL (see e.g. Stull, 1988; Chandra et al., 2010). The occurrence of these turbulent scales in the ground-based EC data indicates that during the period p_1, air very close to the ground is able to be transported upwards very efficiently by non-local large-eddy transport processes. The free convective conditions detected simultaneously by the EC measurements also support these findings. By the onset of the up-valley wind these turbulent scales disappear from the data indicating that the turbulent transport of near-ground air became less effective. The effective vertical transport in period p_1 is important because air masses close to the valley bottom are humid, have a characteristic chemical composition, and may possibly be polluted. The effect of the free convective release of surface layer

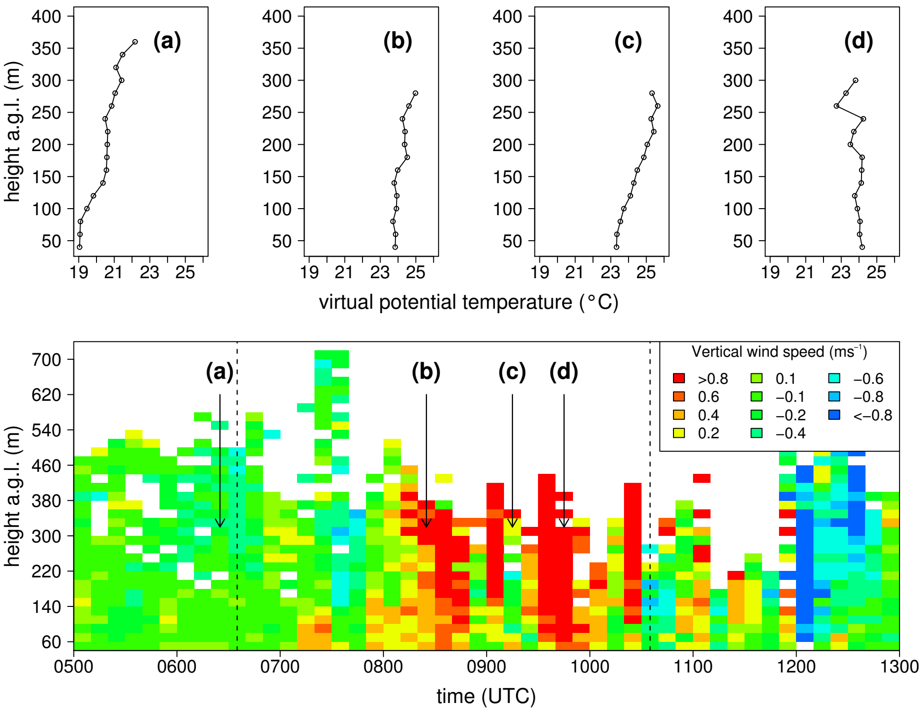

Fig. 4 Upper panel (a-d): Profiles of the virtual potential temperature observed by the Sodar/RASS in the morning hours of COPS IOP15b (13 August 2007). The times of the profiles are marked in the lower panel. Lower panel (from Eigenmann et al., 2009, modified): Vertical wind speeds in colour measured by the Sodar/RASS from 0500-1300 UTC. The black dashed vertical lines indicate the period of vanishing horizontal wind speeds.

air masses from the valley bottom on ozone measurements at a mountain-top station was recently reported by Mayer et al. (2008).

During these free convective situations in period p_1, the Sodar/RASS observed strong vertical updraughts into the stably stratified valley atmosphere. For illustration, Fig. 4 shows for COPS IOP15b, i.e. 13 August 2007, the morning evolution of vertical wind and virtual potential temperature. In the lower panel of Fig. 4 the observed vertical wind is shown from 0500 to 1300 UTC. The period of low horizontal wind speed in the morning is marked by vertical dashed lines. The times of the profiles plotted in Fig. 4a-d are indicated in the lower panel. At time (a) the stable stratification is shown shortly after sunrise. In (b) the profile is representative for a period of strong coherent vertical updraughts. Nearly neutral stratification below 160 m above the valley floor was observed in this period. A weak stable stratification above 160 m can be seen while the corresponding vertical wind speeds remain positive. The strong updraught period is interrupted by a period of weaker vertical winds. The profile in (c) shows that during this short interruption the original stable stratification recovers. After this interruption the vertical wind is again positive and the profile in (d) shows a neutral or slightly unstable profile. In the light of the previous analysis, this individual scene is interpreted as follows: The convection organizes, influenced by the orography, in a way that the updraught and downdraught areas remain quasi-stationary at their spatial location (see Fig. 3). The immobile Sodar/RASS instrument observed this quasi-stationary

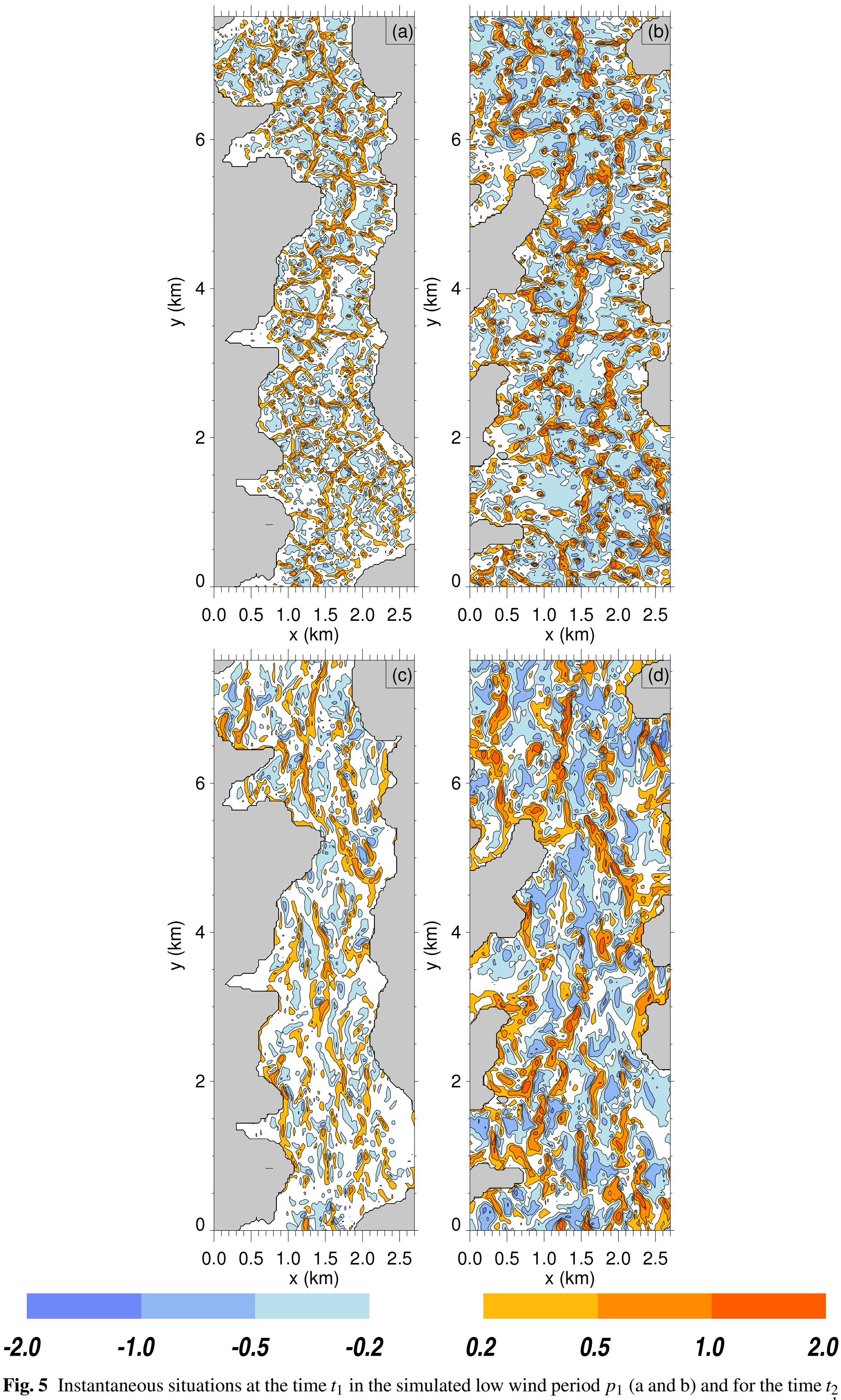

Fig. 5 Instantaneous situations at the time t_1 in the simulated low wind period p_1 (a and b) and for the time t_2 in the simulated up-valley wind period p_2 (c and d) of the simulation $R2$. Vertical wind component w in $\mathrm{m\,s^{-1}}$ is colour-coded. The cross sections are placed at 210 m (a and c) and 300 m a.s.l. (b and d), respectively. The area shown here is marked by the red frame in Fig. 3.

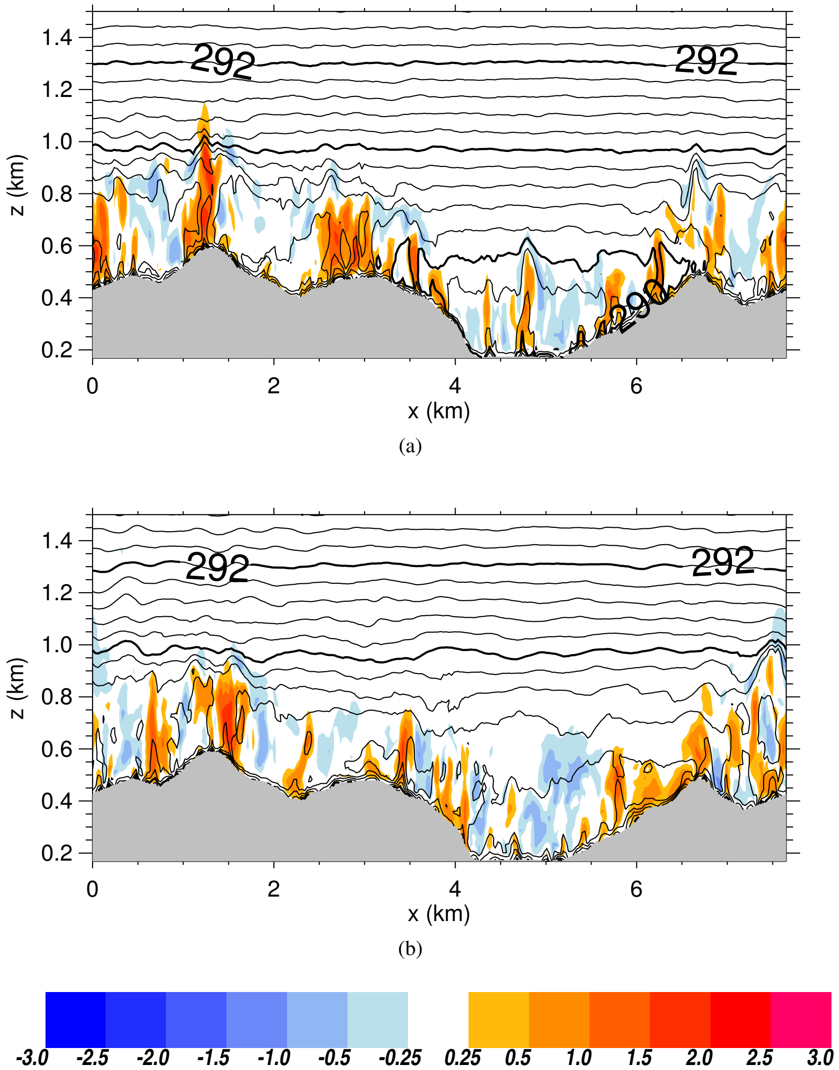

Fig. 6 Vertical cross sections perpendicular to the axis of the valley. Instantaneous situations of the simulation $R2$ are shown for the time t_1 in p_1 (a) and for the time t_2 in p_2 (b). Vertical wind w in m s^{-1} is colour-coded. Black lines are isentropes in steps of 0.2 K. Intersection with the orography is shaded in grey.

updraught area for a period of approximately two and a half hours (0800 until 1030 UTC). This period is interrupted by a short period of weaker winds at around 0920 UTC, when the quasi-stationary updraught area slightly moves out of the view of the Sodar/RASS instrument, so that the properties of an attached downdraught area are also observed. In this short period, it can be seen that the stratification of the valley atmosphere outside of the updraughts is still stable (Fig. 4c).

To better understand the state of the boundary layer in which these observations were made, the transient simulation $R2$ (see Sect. 2.2) was carried out and analysed. In Fig. 5,

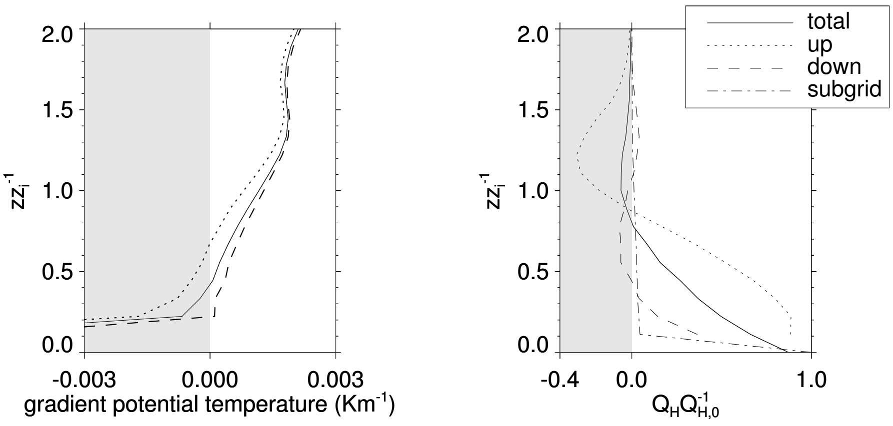

(a) (b)

Fig. 7 (a) Vertical profiles of the gradient of the potential temperature and (b) normalized vertical profiles of the heat flux Q_H at time t_1 of the simulation $R2$. Only points in the valley are considered (see red frame in Fig. 3). The solid line shows the values for all points in the valley. The dotted lines shows the profile for places with $w > 0$ (up) and the dashed line for places with $w < 0$ (down). The contribution to the heat flux from the sub-grid model is shown in (b) as dash-dotted line.

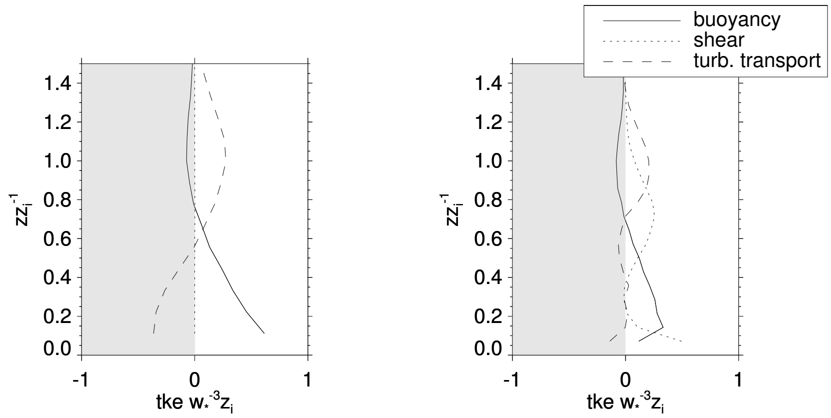

(a) (b)

Fig. 8 Vertical profiles of the TKE budget terms of buoyancy, shear and transport for the time t_1 in p_1 (a) and for the time t_2 in p_2 (b) of the simulation $R2$. Only points in the valley are considered (see red frame in Fig. 3).

snapshots of the field of the vertical wind speed are shown for two heights and for the time t_1 in the low wind speed period p_1 and the time t_2 in the up-valley wind period p_2. Figure 5a and b show - especially in the lower height - the typical spoke patterns at time t_1 (e.g. Schmidt and Schumann, 1989). In contrast, at time t_2 (Fig. 5c, d) there are hardly any of these regular patterns left and instead there are now irregular streak-like patterns. The axis of the streak-like structures is aligned roughly in the main wind direction. Roll or streak-like structures in a shear-buoyancy-driven boundary layer are a well-described phenomena in literature (e.g. Moeng and Sullivan, 1994; Weckwerth et al., 1997; Drobinski et al., 1998; Drobinski and Foster, 2003). The locations of updraughts and downdraughts in the instantaneous snapshots at time t_1 in Fig. 5a and b agree well with those found in the ensemble and time mean in Fig. 3. Figure 6 shows the vertical wind and the temperature stratification for instantaneous vertical slices through the model domain at time t_1 (Fig. 6a) and at time t_2 (Fig. 6b). Similar to the observations shown in Fig. 4, strong convective updraught structures can be seen in period p_1 within the valley which penetrate into the stably stratified free atmosphere up to a height of about 600 m a.s.l. Within a coherent updraught structure a more neutral stratification is found. In period p_2, more neutral stratification can be seen within the entire valley. The vertical extent of the updraught structures is confined to the neutrally stratified valley atmosphere and does not reach into the stably stratified atmosphere above.

The heat flux profiles and the corresponding vertical gradients of the potential temperature in period p_1 are shown in Fig. 7a and Fig. 7b, respectively. The profiles are calculated as horizontal mean for the area marked with the red frame in Fig. 3. Besides the mean profiles within the valley for all points, profiles for updraught and downdraught areas are analysed separately. In the center of the valley boundary layer between about $0.4z_i$ and $0.8z_i$ the flux of sensible heat, averaged horizontally over all points in the valley, is counter to the temperature gradient. Regarding the updraught area, the heat flux follows the temperature gradient up to a height of $0.65z_i$ due to the unstable to neutral stratification. A counter-gradient flux remains above this height up to approximately $0.9z_i$. Counter-gradient fluxes are a common feature in turbulent flows and are well studied (e.g. Schumann, 1987). The counter-gradient turbulent transfer within forest canopies is discussed, e.g., in Denmead and Bradley (1985). The total heat flux is mainly determined by the flux within the coherent upward motions. Together with the findings in Sec. 3.2 (the orography forces the updraught areas to evolve at specific locations), this result leads to the statement that the majority of the flux takes place at these specific locations.

The change of the flow in the periods $p1$ and $p2$ leads to a modified vertical turbulent transport of TKE. Figure 8 shows the profiles of the transport term of the TKE budget for both times t_1 and t_2. At time t_1, the profile of the turbulent transport of TKE shows negative values in the lower half of the boundary layer and positive values in the upper half (Fig. 8a). Due to the vertical orientation of the flow in p_1, the TKE is redistributed vertically by turbulent eddies. At time t_2 (Fig. 8b), the profile of the turbulent transport of TKE deviates strongly from the situation at t_1. Its values are close to zero up to a height of $0.7z_i$. Above this height positive values prevail. This means that the vertical turbulent transport of TKE has ceased in the period p_2. The positive values above $0.7z_i$ originate from the production of TKE from outside the valley, i.e. the averaging area (red frame in Fig. 3).

The profiles for the buoyancy term and the shear term of the TKE budget are plotted in Fig. 8 in the same manner as the profiles described above. During the transition from t_1 to t_2, the profile for buoyancy production of TKE remains positive below $0.7z_i$ and negative above. The major change here is that the maximum of the buoyant production of TKE is shifted upwards to $0.15z_i$. This shift is accompanied by an increased shear production of TKE below $0.2z_i$. The maximum in shear production of TKE at $0.7z_i$ at the time t_2 derives from the imposed along valley wind described in Sec. 2.2.2.

4 Conclusions

During the three months of the COPS campaign the surface energy balance at the site in the Kinzig valley was rarely closed, as common for many energy balance measurements.

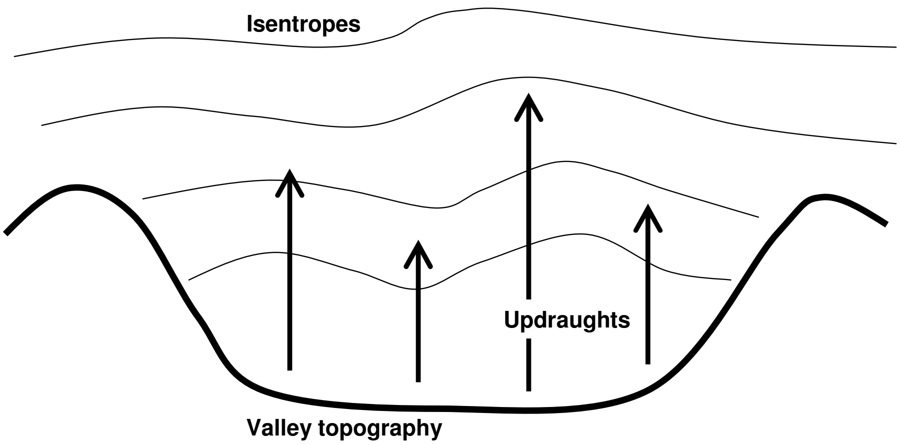

Fig. 9 Schematic view of the turbulent transport during the early-morning low wind speed periods in the Kinzig valley. Strong updraughts exist at specific, preferential locations in the valley which penetrate into the stably stratified valley atmosphere and extend up to about the height of the surrounding ridges.

However, the analysis in this study gave the surprising result that the energy balance was closed on average for the low wind period in the morning hours on radiation days. A closed energy balance indicates that all energy containing motions were captured by the instrumentation and that the assumptions for data processing, i.e. stationarity and homogeneity of the flow, were satisfied. It has to be assumed that due to the vanishing horizontal wind speed no missing advective flux components developed over the complex terrain. After the onset of the valley wind, missing advective flux components occurred and the desired closure was no longer met, with the residual of the energy balance going up to values typical for the full data set of this site. The partition of the turbulent heat flux into the contributions of latent and sensible heat indicated that the residual in the considered data occurs due to the reduced relative sensible heat flux.

Large-eddy simulations of the atmosphere in the Kinzig valley were carried out. It was found that the convection in the valley gets organized by the surrounding ridges during the low-wind period, resulting in quasi-stationary patterns. With this finding the observations of the Sodar/RASS instrument were interpreted in a new way. The distribution of the vertical wind speed, observed by the Sodar/RASS, did not follow the expected pdfs known from literature. While the pdfs derived from the simulations confirmed the results from literature, the pdfs derived from the areas of preferred vertical motion matched well with the observations. This is a strong indication that under the conditions considered here there are orographically induced stationary convection patterns in the valley and further, that the site of the Sodar/RASS was placed in an area of preferred upward motion.

Both the Sodar/RASS observations and the simulations indicate that the turbulent transfer within the valley is counter to the temperature gradient during the early-morning low wind period. This finding is also illustrated schematically in Fig. 9. Surface layer air mass characteristics are transported into higher regions of the stably stratified free atmosphere by strong coherent updraughts in these situations. These coherent updraught structures were shown to occur at specific, preferential locations. The vertical extent of these updraughts happens to be about the height of the surrounding ridges or slightly higher. With the above-valley or large-scale flow at these heights, it can be expected that the vertically transported surface layer air mass characteristics can be translocated horizontally and alter boundary-layer properties elsewhere. As situations of low wind speeds together with high sensible heat fluxes can also develop in different settings of complex terrain (e.g. Hiller et al., 2008; Mayer et al., 2008; Zhou et al., 2011), the observed vertical transport mechanism is not restricted to the conditions in the Kinzig valley. Mayer et al. (2008), e.g., observed the free convective coherent release of surface layer trace gases into upper regions of the boundary layer, which were then advected by the mean wind towards a mountain summit and altered the trace gas observations there significantly. For that reason, the free convective coherent transport of surface layer air mass properties into a stably stratified boundary layer as described in this study should be considered within further boundary-layer experiments.

Acknowledgements This study was funded by the Deutsche Forschungsgesellschaft (DFG) within the special priority program SPP1167 (WI 1685/9-1, WI 1685/10-1, FO 226/19-1, FO 226/23-1). The numerical simulations made for this study were carried out at the high performance computing center of the Deutsches Klima Rechenzentrum (DKRZ) in Hamburg, Germany.

References

Beyrich F (1997) Mixing height estimation from sodar data - A critical discussion. Atmos Environ 31(23):3941–3953, DOI 10.1016/S1352-2310(97)00231-8

Chandra AS, Kollias P, Giangrande SE, Klein SA (2010) Long-term observations of the convective boundary layer using insect radar returns at the SGP ARM climate research facility. J Clim 23(21):5699–5714, DOI 10.1175/2010JCLI3395.1

Charuchittipan D, Babel W, Mauder M, Beyrich F, Leps JP, Foken T (2013) Extension of the averaging time of the eddy-covariance measurement and its effect on the energy balance closure. Boundary-Layer Meteorol to be submitted

Clark T, Farley R (1984) Severe downslope windstorm calculations in 2 and 3 spatial dimensions using anelastic interactive grid nesting - a possible mechanism for gustiness. J Atmos Sci 41(3):329–350, DOI 10.1175/1520-0469(1984)041<0329:SDWCIT>2.0.CO;2

Deardorff J, Willis G (1985) Further results from a laboratory model of the convective planetary boundary layer. Boundary-Layer Meteorol 32:205–236, DOI 10.1007/BF00121880

Deardorff JW (1970) Convective velocity and temperature scales for the unstable planetary boundary layer and for rayleigh convection. J Atmos Sci 27:1211–1213, DOI 10.1175/1520-0469(1970)027<1211:CVATSF>2.0.CO;2

Defant F (1949) Zur Theorie der Hangwinde, nebst Bemerkungen zur Theorie der Berg- und Talwinde. Arch Meteorol Geophys Bioklim A1:421–450

Denmead DT, Bradley EF (1985) Flux-gradient relationships in a forest canopy. In: Hutchison BA, Hicks BB (eds) The forest-atmosphere interaction, D. Reidel Publ. Comp., Dordrecht, Boston, London, pp 421–442

Dörnbrack A, Schumann U (1993) Numerical simulation of turbulent convective flow over wavy terrain. Boundary-Layer Meteorol 65:323–355, DOI 10.1007/BF00707032

Drobinski P, Foster RC (2003) On the origin of near-surface streaks in the neutrally-stratified planetary boundary layer. Boundary-Layer Meteorol 108:247–256, DOI 10.1023/A:1024100125735

Drobinski P, Brown RA, Flamant PH, Pelon J (1998) Evidence of organized large eddies by ground-based doppler lidar, sonic anemometer and sodar. Boundary-Layer Meteorol 88:343–361, DOI 10.1023/A:1001167212584

Eigenmann R, Metzger S, Foken T (2009) Generation of free convection due to changes of the local circulation system. Atmos Chem Phys 9:8587–8600, DOI 10.5194/acp-9-8587-2009

Eigenmann R, Kalthoff N, Foken T, Dorninger M, Kohler M, Legain D, Pigeon G, Piguet B, Schüttemeyer D, Traulle O (2011) Surface energy balance and turbulence network during the Convective and Orographically-induced Precipitation Study (COPS). Q J Roy Meteorol Soc 137(S1):57–69, DOI 10.1002/qj.704

Foken T (2008) The energy balance closure problem: An overview. Ecol Appl 18:1351–1367, DOI 10.1890/06-0922.1

Foken T, Mauder M, Liebethal C, Wimmer F, Beyrich F, Leps JP, Raasch S, DeBruin HAR, Meijninger WML, Bange J (2010) Energy balance closure for the LITFASS-2003 experiment. Theor Appl Climatol 101:149–160, DOI 10.1007/s00704-009-0216-8

Foken T, Aubinet M, Finnigan JJ, Leclerc MY, Mauder M, Paw U KT (2011) Results of a panel discussion about the energy balance closure correction for trace gases. Bull Am Meteorol Soc 92:ES13–ES18, DOI 10.1175/2011BAMS3130.1

Foken T, Aubinet M, Leuning R (2012) The eddy covariance method. In: Aubinet M, Vesala T, Papale D (eds) Eddy Covariance, Springer Atmospheric Sciences, Springer Netherlands, pp 1–19, DOI 10.1007/978-94-007-2351-1-1

Gal-Chen T, Somerville RC (1975) On the use of a coordinate transformation for the solution of the Navier-Stokes equations. J Comput Phys 17:209 – 228, DOI 10.1016/0021-9991(75)90037-6

Hiller R, Zeeman M, Eugster W (2008) Eddy-covariance flux measurements in the complex terrain of an alpine valley in switzerland. Boundary-Layer Meteorol 127:449–467, DOI 10.1007/s10546-008-9267-0

Inagaki A, Letzel MO, Raasch S, Kanda M (2006) Impact of surface heterogeneity on energy imbalance: A study using LES. J Meteorol Soc Jpn 84:187–198, DOI 10.2151/jmsj.84.187

Kalthoff N, Kohler M, Barthlott C, Adler B, Mobbs S, Corsmeier U, Träumner K, Foken T, Eigenmann R, Krauss L, Khodayar S, Di Girolamo P (2011) The dependence of convection-related parameters on surface and boundary-layer conditions over complex terrain. Q J Roy Meteorol Soc 137(S1):70–80, DOI 10.1002/qj.686

Kanda M, Moriwaki R, Kasamatsu F (2004) Large-eddy simulation of turbulent organized structures within and above explicitly resolved cube arrays. Boundary-Layer Meteorol 112(2):343–368, DOI 10.1023/B:BOUN.0000027909.40439.7c

Kühnlein C, Smolarkiewicz PK, Dörnbrack A (2012) Modelling atmospheric flows with adaptive moving meshes. J Comput Phys 231(7):2741–2763, DOI 10.1016/j.jcp.2011.12.012

Mahrt L (2010) Computing turbulent fluxes near the surface: Needed improvements. Agric For Meteorol 150(4):501–509, DOI 10.1016/j.agrformet.2010.01.015

Mauder M, Foken T (2006) Impact of post-field data processing on eddy covariance flux estimates and energy balance closure. Meteorol Z 15(6):597–609, DOI doi:10.1127/0941-2948/2006/0167

Mayer JC, Staudt K, Gilge S, Meixner FX, Foken T (2008) The impact of free convection on late morning ozone decreases on an Alpine foreland mountain summit. Atmos Chem Phys 8:5941–5956, DOI 10.5194/acp-8-5941-2008

Metzger S, Foken T, Eigenmann R, Kurtz W, Serafimovich A, Siebicke L, Olesch J, Staudt K, Lüers J (2007) COPS experiment, Convective and orographically induced precipitation study, 01 June 2007 – 31 August 2007, Documentation. Work Report University of Bayreuth, Department of Micrometeorology, 34, Print: ISSN 1614-8916, 72 pp.

Moeng CH, Sullivan PP (1994) A comparison of shear- and buoyancy-driven planetary boundary layer flows. J Atmos Sci 51:999–1022, DOI 10.1175/1520-0469(1994)051<0999:ACOSAB>2.0.CO;2

NASA Land Processes Distributed Active Archive Center NASA LP DAAC (2001) ASTGTM ASTER Global Digital Elevation Model. LP DAAC, USGS/Earth Resources Observation and Science (EROS) Center, Sioux Falls, South Dakota.

Oncley SP, Foken T, Vogt R, Kohsiek W, DeBruin HAR, Bernhofer C, Christen A, van Gorsel E, Grantz D, Feigenwinter C, Lehner I, Liebethal C, Liu H, Mauder M, Pitacco A, Ribeiro L, Weidinger T (2007) The Energy Balance Experiment EBEX-2000. Part I: Overview and energy balance. Boundary-Layer Meteorol 123:1–28, DOI 10.1007/s10546-007-9161-1

Piotrowski Z, Smolarkiewicz P, Malinowski S, Wyszogrodzki A (2009) On numerical realizability of thermal convection. J Comput Phys 228:6268–6290, DOI 10.1016/j.jcp.2009.05.023

Prusa JM, Smolarkiewicz PK (2003) An all-scale anelastic model for geophysical flows: dynamic grid deformation. J Comput Phys 190:601 – 622, DOI 10.1016/S0021-9991(03)00299-7

Prusa JM, Smolarkiewicz PK, Wyszogrodzki AA (2008) Eulag, a computational model for multiscale flows. Comput Fluids 37(9):1193–1207, DOI 10.1016/J.Compfluid.2007.12.001

Raasch S, Harbusch G (2001) An analysis of secondary circulations and their effects caused by small-scale surface inhomogeneities using large-eddy simulation. Boundary-Layer Meteorol 101:31–59, DOI 10.1023/A:1019297504109

Rotach MW, Andretta M, Calanca P, Weigel AP, Weiss A (2008) Boundary layer characteristics and turbulent exchange mechanisms in highly complex terrain. Acta Geophys 56(1):194–219, DOI 10.2478/s11600-007-0043-1

Schmidt H, Schumann U (1989) Coherent structure of the convective boundary layer derived from large-eddy simulations. J Fluid Mech 200:511–562, DOI 10.1017/S0022112089000753

Schumann U (1987) The countergradient heat flux in turbulent stratified flows. Nucl Eng Des 100(3):255–262, DOI 10.1016/0029-5493(87)90078-1

Segal M, Arritt RW (1992) Nonclassical mesoscale circulations caused by surface sensible heat-flux gradients. Bull Am Meteorol Soc 73(10):1593–1604, DOI 10.1175/1520-0477(1992)073<1593:NMCCBS>2.0.CO;2

Smolarkiewicz PK, Margolin LG (1993) On forward-in-time differencing for fluids: Extension to a curvilinear framework. Mon Weather Rev 121(6):1847–1859, DOI 10.1175/1520-0493(1993)121<1847:OFITDF>2.0.CO;2

Smolarkiewicz PK, Margolin LG (1998) MPDATA: a finite-difference solver for geophysical flows. J Comput Phys 140(2):459–480, DOI 10.1006/jcph.1998.5901

Smolarkiewicz PK, Grubisic V, Margolin LG (1997) On forward-in-time differencing for fluids: Stopping criteria for iterative solutions of anelastic pressure equations. Mon Weather Rev 125(4):647–654, DOI 10.1175/1520-0493(1997)125<0647:OFITDF>2.0.CO;2

Smolarkiewicz PK, Sharman R, Weil J, Perry SG, Heist D, Bowker G (2007) Building resolving large-eddy simulations and comparison with wind tunnel experiments. J Comput Phys 227:633–653, DOI 10.1016/j.jcp.2007.08.005

Sorbjan Z (1996) Numerical study of penetrative and ”solid lid” nonpenetrative convective boundary layers. J Atmos Sci 53:101–112, DOI 10.1175/1520-0469(1996)053<0101:NSOPAL>2.0.CO;2

Stoy P, Mauder M, Foken T, Marcolla B, Boegh E, Ibrom A, Arain M, Arneth A, Aurela M, Bernhofer C, Cescatti A, Dellwik E, Duce P, Gianelle D, van Gorsel E, Kiely G, Knohl A, Mangolis H, McCaughey H, Merbold L, Montagnani L, Papale D, Reichstein M, Serrano-Ortiz P, Sottocornola M, Saunders M, Spano D, Vaccari F, Varlagin A (2013) A data-driven analysis of energy balance closure across FLUXNET research sites: The role of landscape-scale heterogeneity. Agric For Meteorol , accepted

Stull RB (1988) An introduction to boundary layer meteorology. Kluwer Academic Publishers, Dordrecht

Thomas SJ, Hacker JP, Smolarkiewicz PK, Stull RB (2003) Spectral preconditioners for nonhydrostatic atmospheric models. Mon Weather Rev 131(10):2464–2478, DOI 10.1175/1520-0493(2003)131<2464:SPFNAM>2.0.CO;2

Twine TE, Kustas WP, Norman JM, Cook DR, Houser PR, Meyers TP, Prueger JH, Starks PJ, Wesely ML (2000) Correcting eddy-covariance flux underestimates over a grassland. Agric For Meteorol 103:279–300

Walko R, Cotton W, Pielke R (1992) Large-eddy simulations of the effects of hilly terrain on the convective boundary-layer. Boundary-Layer Meteorol 58(1-2):133–150, DOI 10.1007/BF00120755

Weckwerth TM, Wilson JW, Wakimoto RM, Crook NA (1997) Horizontal convective rolls: determining the environmental conditions supporting their existence and characteristics. Mon Weather Rev 125:505–526, DOI 10.1175/1520-0493(1997)125<0505:HCRDTE>2.0.CO;2

Wedi NP, Smolarkiewicz PK (2004) Extending Gal-Chen and Somerville terrain-following coordinate transformation on time-dependent curvilinear boundaries. J Comput Phys 193:1–20, DOI 10.1016/j.jcp.2003.07.034

Weigel A, Chow F, Rotach M (2007) The effect of mountainous topography on moisture exchange between the ”surface” and the free atmosphere. Boundary-Layer Meteorol 125:227–244, DOI 10.1007/s10546-006-9120-2

Whiteman CD (1990) Observations of thermally developed wind systems in mountainous terrain. In: Blumen W (ed) Atmospheric processes over complex terrain, Meteorological monographs, vol 23 (45), American Meteorological Society, Boston, Massachusetts, pp 5–42

Whiteman CD (2000) Mountain Meteorology: Fundamentals and Applications. Oxford University Press, USA

Wulfmeyer V, Behrendt A, Kottmeier C, Corsmeier U, Barthlott C, Craig GC, Hagen M, Althausen D, Aoshima F, Arpagaus M, Bauer HS, Bennett L, Blyth A, Brandau C, Champollion C, Crewell S, Dick G, Di Girolamo P, Dorninger M, Dufournet Y, Eigenmann R, Engelmann R, Flamant C, Foken T, Gorgas T, Grzeschik M, Handwerker J, Hauck C, Höller H, Junkermann W, Kalthoff N, Kiemle C, Klink S, König M, Krauss L, Long CN, Madonna F, Mobbs S, Neininger B, Pal S, Peters G, Pigeon G, Richard E, Rotach MW, Russchenberg H, Schwitalla T, Smith V, Steinacker R, Trentmann J, Turner DD, van Baelen J, Vogt S, Volkert H, Weckwerth T, Wernli H, Wieser A, Wirth M (2011) The Convective and Orographically-induced Precipitation Study (COPS): the scientific strategy, the field phase, and research highlights. Q J Roy Meteorol Soc 137(S1):3–30, DOI 10.1002/qj.752

Zardi D, Whiteman CD (2013) Diurnal mountain wind systems. In: Chow FK, De Wekker SF, Snyder BJ (eds) Mountain Weather Research and Forecasting, Springer Netherlands, Dordrecht, pp 35–119

Zhou D, Eigenmann R, Babel W, Foken T, Ma Y (2011) The study of near-ground free convection conditions at nam co station on the tibetan plateau. Theor Appl Climatol 105:217–

228, DOI 10.1007/s00704-010-0393-5